Response of Insulated Electric Field Probes in Finite Heterogeneous Biological Bodies

SEYED HOSSEIN MOUSAVINEZHAD, MEMBER, IEEE, KUN-MU CHEN, FELLOW, IEEE, AND DENNIS PAUL NYQUIST, MEMBER, IEEE

Abstract—**An ideal probe for measuring the electric field inside a finite heterogeneous biological body should possess a constant calibration factor; probe effective length and equivalent impedance must therefore be independent of its location in the body. A practical probe with minimal variation of these parameters can be implemented by insulating the metallic probe with a thick low-loss dielectric coating of low permittivity. An idealized spherical probe, insulated by a dielectric layer and immersed in a finite lossy-dielectric body (representative of more general probes) is studied. Analytical expressions for the effective diameter and equivalent impedance of the probe are obtained. Numerical results indicate that the variation of these parameters with probe location is minimized by coating the probe with a relatively thick low-permittivity dielectric layer. Experimental impedance and electric field measurements confirm this conclusion. Limitation of using this probe in biological media with low dielectric constants is discussed.**

I. Introduction

TO ACCURATELY ASSESS the potential biological hazard associated with electromagnetic (EM) radiation, it is necessary to determine the EM field induced inside a finite biological body or a phantom model of that body [1]–[3]. Electric field probes are frequently used in bioeffects research to measure the field excited in a finite heterogeneous biological body due to its interaction with a (generally nonuniform) impressed EM field [4]–[9]. The response of an ideal probe is proportional to the induced $\vec{E}$ field at its location in the body and independent of any body inhomogeneity, i.e., its calibration factor does not depend upon finite body dimensions or local variations of its electrical parameters. The properties of an insulated antenna in an unbounded lossy medium have also been studied [10].

It has been demonstrated [7] that the equivalent circuit parameters (calibration factors) of practical probes in general vary with the location of the probe in a finite heterogeneous biological body. The probe effective length can be strongly influenced by body permittivity and conductivity at its location, while the probe equivalent impedance is sensitive to both finite body dimensions and electrical heterogeneity. Calibration factor variations resulting from these location-dependent equivalent circuit parameters have been identified [7] as the cause for discrepancies between theoretically predicted and experimentally measured electric fields as a dipole-type probe approaches the boundaries of simulated biological bodies consisting of a finite volume of saline solution. It is the purpose of this paper to demonstrate that these location-dependent probe parameter variations can be reduced by insulating the metallic probe with a thick coating of low-permittivity dielectric.

In the interest of obtaining relatively simple, but generally representative closed-form results, an idealized spherical metallic probe insulated by a dielectric layer and immersed in a finite lossy-dielectric biological body (each spherical and concentric with the probe) is studied. Analytical expressions for the effective diameter d_{eff} and equivalent impedance Z_{eq} of the probe are determined in terms of the radii and electrical parameters of the insulating layer and the finite body. Theoretically predicted impedances Z_{eq} compare will with experimentally measured values. Numerical results are presented from which it is concluded that variations of probe equivalent circuit parameters d_{eff} and Z_{eq} (calibration factor) are minimized by coating the probe with a relatively thick insulating layer of low permittivity. Comparison of theoretically calculated induced power density distributions with those measured by an insulated spherical probe immersed in a finite volume of saline solution display excellent agreement at all locations in the solution. This correspondence confirms the above conclusions regarding the relative calibration factor constancy for the insulated probe.

In this study, it was found that an implantable electric field probe may not perform well in biological tissues with low dielectric constants.

II. Decomposition into Scattering and Radiating Modes—Probe Equivalent Circuit

The geometrical configuration of the insulated spherical probe is indicated in Figs. 1(a) and (b). A metallic sphere of radius a is centered at the origin of spherical coordinates and loaded by impedance Z across an equatorial gap (angular width $2\theta_0$ as shown in Fig. 7) at $\theta = \pi/2$. The probe is insulated by a concentric spherical dielectric

Manuscript received August 22, 1977; revised March 12, 1978. This work was supported in part by the U.S. Army Research Office under Grant DAAG29-76-G-0201.

S. H. Mousavinezhad was with the Department of Electrical Engineering and Systems Science, Michigan State University, East Lansing, MI. He is now with the School of Engineering, Ferdowsi University, Mashhad, Iran.

K. M. Chen and D. P. Nyquist are with the Department of Electrical Engineering and Systems Science, Michigan State University, East Lansing, MI 48824.

0018-9480/78/0800-0599$00.75

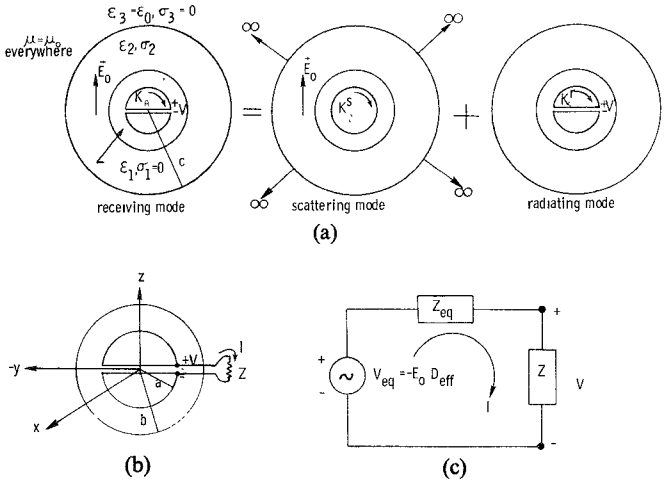

Fig. 1. Configuration of insulated spherical probe, modal decomposition, equivalent circuit. (a) Decomposition of probe receiving mode into superposition of scattering and radiating modes. (b) Detail of loaded insulated probe. (c) Probe equivalent circuit.

layer (region 1: $a<r<b$: ϵ_1, $\sigma_1=0$) of radius b and immersed in a concentric spherical biological body (region 2: $b<r<c$; ϵ_2, σ_2) of finite radius c. The biological body is immersed in free space (region 3: $c<r<\infty$; $\epsilon_3=\epsilon_0$, $\sigma_3=0$). Each region is nonmagnetic with $\mu=\mu_0$.

It is assumed that the field to be measured in the body at the location of the probe is $\vec{E}_0$. Impressed field $\vec{E}_0$ is

$$\vec{E}_0=\hat{z}E_0=\hat{r}E_0\cos\theta-\hat{\theta}E_0\sin\theta \tag{1}$$

and this field excites surface current $\vec{K}=\hat{\theta}K_\theta$ on the metallic sphere; it follows from Maxwell's equations that the EM field in each of the three regions ($l=1,2,3$) takes the form

$$\begin{aligned}\vec{E}_l(r,\theta)&=\hat{r}E_{lr}(r,\theta)+\hat{\theta}E_{l\theta}(r,\theta)\\ \vec{H}_l(r,\theta)&=\hat{\phi}H_{l\phi}(r,\theta).\end{aligned} \tag{2}$$

The response of the probe in its receiving mode can be decomposed into the superposition of a scattering mode and a radiating mode as indicated in Fig. 1(a). Total surface current excited on the metallic sphere can be expressed as

$$K_\theta(\theta)=K_\theta^s(\theta)+K_\theta^r(\theta) \tag{3}$$

while tangential components of total EM fields in each region take the form

$$\begin{aligned}E_{l\theta}(r,\theta)&=E_{l\theta}^s(r,\theta)+E_{l\theta}^r(r,\theta)\\ H_{l\phi}(r,\theta)&=H_{l\phi}^s(r,\theta)+H_{l\phi}^r(r,\theta)\end{aligned} \tag{4}$$

where superscripts s and r designate the scattering and radiating modes, respectively. Field $\vec{E}_0$ in the body, which excites the probe, is presumed known and the EM field scattered by the metallic sphere attenuates rapidly in the semiconducting body; to obtain a tractable solution, it is therefore assumed for the scattering mode that the biological body is of infinite extent. Effects of finite body dimensions (on probe impedance) are retained for the radiating mode.

With an assumed $e^{j\omega t}$ harmonic time dependence, Maxwell's equations lead to a wave equation for the magnetic field in each region as

$$\nabla\times\nabla\times\vec{H}_l^p-k_l^2\vec{H}_l^p=0 \tag{5}$$

where $l=1,2,3$ designates the various regions and $p=s,r$ designates fields of the scattering and radiating modes with

$k_l=\omega\sqrt{\mu_0\xi_l}$ = wavenumber in lth region
$\eta_l=\sqrt{\mu_0/\xi_l}$ = wave impedance in lth region
$\xi_l=\epsilon_l-j\sigma_l/\omega$ = equivalent complex permittivity of lth region.

Solutions to wave equation (5) for the magnetic field can be constructed as spherical eigenmode expansions [11]; electric fields $\vec{E}_l^p$ are subsequently obtained from Maxwell's equations such that tangential EM field components are expressed in the form

$$\begin{aligned}H_{l\phi}^p(r,\theta)&=\sum_{n=1}^{\infty}\left[H_{l\phi n}^{p+}(r)+H_{l\phi n}^{p-}(r)\right]p_n^1(\cos\theta)\\ E_{l\theta}^p(r,\theta)&=\sum_{n=1}^{\infty}\left[Z_{ln}^{+}(r)H_{l\phi n}^{p+}(r)-Z_{ln}^{-}(r)H_{l\phi n}^{p-}(r)\right]p_n^1(\cos\theta)\end{aligned} \tag{6}$$

where p_n^1 is the associated Legendre function and

$$H_{l\phi n}^{p+}(r)=\frac{A_{ln}^pH_{n+1/2}^{(2)}(k_lr)}{\sqrt{k_lr}},\quad H_{l\phi n}^{p-}(r)=\frac{B_{ln}^pH_{n+1/2}^{(1)}(k_lr)}{\sqrt{k_lr}} \tag{7}$$

$$Z_{ln}^{+}(r)=j\eta_l\left[\frac{H_{n-1/2}^{(2)}(k_lr)}{H_{n+1/2}^{(2)}(k_lr)}-\frac{n}{k_lr}\right]$$

$$Z_{ln}^{-}(r)=j\eta_l\left[\frac{H_{n-1/2}^{(1)}(k_lr)}{H_{n+1/2}^{(1)}(k_lr)}-\frac{n}{k_lr}\right]. \tag{8}$$

$H_{n\pm1/2}^{(1)}$ and $H_{n\pm1/2}^{(2)}$ are Hankel functions with complex argument [12] while A_{ln}^p and B_{ln}^p are unknown mode amplitude coefficients to be evaluated using appropriate boundary conditions for tangential field components of scattering and radiating modes ($p=s,r$) at interface surfaces between media in the three regions ($l=1,2,3$). $H_{l\phi n}^{p+}$ and $H_{l\phi n}^{p-}$ are outgoing and incoming spherical waves, respectively, while Z_{ln}^{+} and Z_{ln}^{-} are corresponding TM wave impedances.

Details of field solutions for the scattering and radiating modes are subsequently presented in Sections III and IV. Currents of the two modes induced on the surface of the metallic sphere are superposed here to obtain equivalent circuit parameters describing the insulated probe. Total induced surface current is, from (3), $K_\theta(\theta)=K_\theta^s(\theta)+K_\theta^r(\theta)$, evaluating at $\theta=\pi/2$ and multiplying by $2\pi a$ leads to a relation in terms of total currents at the probe

terminals in the form $I = I^s - I^r$ with

$$I = 2\pi a K_\theta(\pi/2) = \frac{V}{Z}$$
$$= \text{load current in receiving probe,}$$
$$I^s = 2\pi a K_\theta^s(\pi/2) = 2\pi a Y(\pi/2) E_0$$
$$= \text{total current in scattering mode,}$$
$$I^r = -2\pi a K_\theta^r(\pi/2) = \frac{V}{Z_{in}}$$
$$= \text{input current to radiating mode}$$

where $K_\theta^s(\theta) = E_0 Y(\theta)$ as developed in Section III and Z_{in} is the input impedance to the radiating mode as expressed in Section IV. The above expressions lead to

$$I = 2\pi a Y(\pi/2) E_0 - \frac{IZ}{Z_{in}} \tag{9}$$

which is solved for load current I and expressed in the form

$$I = \frac{V_{eq}}{Z_{eq} + Z} \tag{10}$$

where

$$V_{eq} = 2\pi a Y(\pi/2) Z_{in} E_0 = -D_{eff} E_0$$
$$= \text{equivalent probe voltage} \tag{11}$$
$$Z_{eq} = Z_{in} = \text{equivalent probe impedance.} \tag{12}$$

Expressions for $Y(\theta)$ and Z_{in} are developed in Sections III and IV (equations (19) and (26)). D_{eff} is the effective probe diameter such that $V_{eq} = -D_{eff} E_0$ and can be expressed in normalized form as

$$d_{eff} = \frac{D_{eff}}{2a} = -\frac{V_{eq}}{2aE_0} = -\pi Z_{in} Y(\pi/2)$$
$$= \text{normalized effective diameter.} \tag{13}$$

d_{eff} is, in general, a complex parameter; numerical results for small probes indicate that $d_{eff} \approx 0.5$. Equation (10) clearly leads to the probe equivalent circuit of Fig. 1(c) with parameters V_{eq} and Z_{eq}.

Probe response (induced voltage across load impedance Z) is specified by

$$V = ZI = KE_0$$
$$K = -\frac{ZD_{eff}}{Z_{eq} + Z} = \text{probe calibration coefficient.} \tag{14}$$

Note that $Z_{eq} = Z_{in}$ of the radiating mode. Clearly, if probe calibration factor K is to be independent of probe location in a finite heterogeneous body, then variations of D_{eff} and Z_{eq} should be minimized. Extensive numerical results and experimental measurements for D_{eff} and Z_{eq} are presented and compared in Section V.

III. Fields of Scattering Mode—Effective Diameter

In the scattering mode of Fig. 1(a), the biological body recedes to infinite radius and only regions 1 and 2 (insulation and body) are present. Appropriate boundary conditions on tangential EM fields in these regions are $E_{1\theta}^s(r = a) = 0$, $E_{1\theta}^s(r = b) = E_{2\theta}^s(r = b) - E_0 \sin\theta$, $H_{1\phi}^s(r = b) = H_{2\phi}^s(r = b)$, and $E_{2\theta}^s(r \to \infty) = 0$. Applying these boundary conditions with the fields of (6) and exploiting orthogonality of the Legendre functions leads to the system of algebraic equations

$$Z_{1n}^+(a) H_{1\phi n}^{s+}(a) - Z_{1n}^-(a) H_{1\phi n}^{s-}(a) = 0$$
$$H_{1\phi n}^{s+}(b) + H_{1\phi n}^{s-}(b) = H_{2\phi n}^{s+}(b)$$
$$Z_{1n}^+(b) H_{1\phi n}^{s+}(b) - Z_{1n}^-(b) H_{1\phi n}^{z-}(b) = Z_{2n}^+(b) H_{2\phi n}^{s+}(b) - E_0 \delta_{1n} \tag{15}$$

for $n = 1, 2, , \cdots, \infty$ where δ_{1n} is the Kronecker δ-function and coefficients A_{1n}^s, B_{1n}^s, and A_{2n}^s are the unknown quantities in this system. Nonzero solutions are obtained only for $n = 1$, i.e., the uniform impressed electric field E_0 excites only the first-order scattering mode in the probe-body system. If the coefficients are normalized to E_0, then the magnetic field at the surface of the metallic sphere can be expressed as

$$H_{1\phi}^s(a, \theta) = E_0 \left[a_{11}^s \frac{H_{3/2}^{(2)}(k_1 a)}{\sqrt{k_1 a}} + b_{11}^s \frac{H_{3/2}^{(1)}(k_1 a)}{\sqrt{k_1 a}} \right] \sin\theta \tag{16}$$

where a_{11}^s and b_{11}^s are normalized solutions to the system (15) with $n = 1$; these are obtained as

$$b_{11}^s = \frac{\sqrt{k_1 b}}{[Z_{21}^+(b) + Z_{11}^-(b)] H_{3/2}^{(1)}(k_1 b) + [Z_{21}^+(b) - Z_{11}^+(b)] \alpha(a) H_{3/2}^{(2)}(k_1 b)}$$

$$a_{11}^s = \alpha(a) b_{11}^s$$
$$\alpha(a) = \frac{Z_{11}^-(a) H_{3/2}^{(1)}(k_1 a)}{Z_{11}^+(a) H_{3/2}^{(2)}(k_1 a)}. \tag{17}$$

The surface current of the scattering mode which is excited on the metallic sphere is $\vec{K}^s = \hat{r} x \vec{H}_1^s(r = a) = -\hat{\theta} H_{1\phi}^s(a, \theta)$ which leads to

$$K_\theta^s(\theta) = E_0 Y(\theta) \tag{18}$$

where

$$Y(\theta) = -\left[a_{11}^s \frac{H_{3/2}^{(2)}(k_1 a)}{\sqrt{k_1 a}} + b_{11}^s \frac{H_{3/2}^{(1)}(k_1 a)}{\sqrt{k_1 a}} \right] \sin\theta. \tag{19}$$

Note that $Y(\theta)$ is dimensionally an admittance function.

IV. Fields of Radiating Mode—Equivalent Impedance

A closed-form analytical expression for the input impedance to a dielectric-coated spherical antenna embedded in a finite conducting body is developed in this section. The configuration of the spherical probe antenna in this radiating mode is indicated in Fig. 1(a); surface current K_θ^r is excited on the metallic sphere by potential V maintained across an equatorial gap of angular width $2\theta_0$ at $\theta=\pi/2$.

Appropriate field solutions for this radiating mode are given by (6) with $p=r$ for each of the three regions ($l=1,2,3$). Since region 3 is unbounded free space, then only an outgoing wave exists in that region and $B_{3n}^r=0$. Five unknown amplitude coefficients (A_{ln}^r for $l=1,2,3$ and B_{ln}^r for $l=1,2$) remain to be determined for each mode n by application of boundary conditions on tangential field components. At the surface ($r=a$) of the conducting sphere, an appropriate boundary condition [13] is $E_{1\theta}^r(r=a^+,\theta)=E_\theta^r(r=a^-,\theta)=(V/a)\delta(\theta-\pi/2)$, while at the dielectric–body and body–vacuum ($r=b,c$) interfaces, it is required that $E_{1\theta}^r(r=b)=E_{2\theta}^r(r=b)$, $H_{1\phi}^r(r=b)=H_{2\phi}^r(r+b)$, $E_{2\theta}^r(r=c)=E_{3\theta}^r(r=c)$, and $H_{2\phi}^r(r=c)=H_{3\phi}^r(r=c)$. The conventional matrix formulation of this boundary-value problem was unsuccessful due to numerical difficulties associated with inversion of nearly singular matrices and the resulting necessity to compute Hankel functions of small complex arguments [14] very accurately. An alternative method, based on transmission line theory, is therefore adopted.

Tangential electric field at the surface of the metallic sphere is first expanded in a Legendre series as

$$E_{1\theta}^r(a,\theta)=\sum_{n=1}^{\infty} F_n p_n^1(\cos\theta)=\frac{V}{a}\delta\left(\theta-\frac{\pi}{2}\right). \tag{20}$$

Expansion coefficients F_n are evaluated by exploiting the orthogonality of Legendre functions p_n^1 [12] to obtain

$$F_n=\frac{V}{a}p_n^1(0)\frac{2n+1}{2n(n+1)}. \tag{21}$$

Since $p_n^1(0)=0$ for even integers n, then the sum in (20) need be extended only over odd integers $n=1,3,1.5,\cdots,\infty$. A system of algebraic equations for the five unknown amplitude coefficients is obtained by substituting appropriate field solutions for $E_{l\theta}^r$ and $H_{l\phi}^r$ from (6) into (20) as well as the boundary conditions at $r=b,c$ and again exploiting the orthogonality of the p_n^1 functions.

A transmission-line formulation for the solution of this boundary-value problem is initiated by defining reflection and transmission coefficients at the interfaces. For example, at $r=b$

$$R_{1n}(b)\equiv\frac{H_{1\phi n}^{r-}(b)}{H_{1\phi n}^{r+}(b)} \qquad T_{1n}(b)\equiv\frac{H_{2\phi n}^{r+}(b)}{H_{1\phi n}^{r+}(b)} \tag{22}$$

while $R_{2n}(c)$ and $T_{2n}(c)$ are defined similarly at $r=c$. Two additional reflection coefficients are defined at $r=a$ and $r=b$ as

$$R_{2n}(b)\equiv\frac{H_{2\phi n}^{r+}(b)}{H_{2\phi n}^{r-}(b)} \qquad R_{1n}(a)\equiv\frac{H_{1\phi n}^{r+}(a)}{H_{1\phi n}^{r-}(a)}. \tag{23}$$

Each of these coefficients is an unknown quantity because $H_{1\phi n}^{r+}$, $H_{1\phi n}^{r-}$, etc., depend upon unknown amplitude coefficients A_{ln}^r and B_{ln}^r. Products of reflection coefficients, however, are known; in terms of the spherical wave definitions these products lead to

$$R_{1n}(a)R_{1n}(b)=\frac{H_{n+1/2}^{(2)}(k_1a)H_{n+1/2}^{(1)}(k_1b)}{H_{n+1/2}^{(1)}(k_1a)H_{n+1/2}^{(2)}(k_1b)}\equiv\frac{1}{K_{1n}(a,b)}$$

$$R_{2n}(b)R_{2n}(c)=\frac{H_{n+1/2}^{(2)}(k_2b)H_{n+1/2}^{(1)}(k_2c)}{H_{n+1/2}^{(1)}(k_2b)H_{n+1/2}^{(2)}(k_2c)}\equiv\frac{1}{K_{2n}(b,c)}. \tag{24}$$

Applying these definitions in the system of equations arising from enforcing boundary conditions at $r=a,b,c$, expressions for $R_{1n}(b)$ and $R_{2n}(c)$ are obtained as [14]

$$R_{1n}(b)=\frac{Z_{1n}^+(b)-QZ_{2n}^+(b)}{Z_{1n}^-(b)+QZ_{2n}^+(b)}$$

$$R_{2n}(c)=\frac{Z_{2n}^+(c)-Z_{3n}^+(c)}{Z_{2n}^-(c)+Z_{3n}^+(c)}$$

$$Q\equiv\frac{1-K_{2n}(b,c)R_{2n}(c)Z_{2n}^-(b)/Z_{2n}^+(b)}{1+K_{2n}(b,c)R_{2n}(c)} \tag{25}$$

where $Z_{1n}^+(b)$, $Z_{1n}^-(b)$, etc., are the TM wave impedances defined in (8).

Total radiating-mode input current excited by potential V at the edge ($r=a$, $\theta=\pi/2-\theta_0$; see Figs. 1(a) and 7) of the spherical antenna is evaluated as [13]

$$I^r=2\pi a\cos\theta_0 K_\theta^r(\theta=\pi/2-\theta_0)=2\pi a\cos\theta_0 H_{1\phi}^r(a,\pi/2-\theta_0)$$

where $H_{1\phi}^r$ is calculated from field expression (6) using known values (21) for expansion coefficients F_n and relations (24) and (25) for reflection coefficients. Input admittance to the insulated spherical probe antenna is finally obtained as

$$(Z_{\text{in}})^{-1}\equiv\frac{I^r}{V}=\cos\theta_0\sum_{\substack{n=1\\(\text{odd})}}^{\infty}\frac{\pi(2n+1)}{n(n+1)}P_n^1(\sin\theta_0)P_n^1(0)$$

$$\cdot\frac{1+K_{1n}(a,b)R_{1n}(b)}{Z_{1n}^+(a)-K_{1n}(a,b)R_{1n}(b)Z_{1n}^-(a)}. \tag{26}$$

This expression yields $A_{\text{eq}}=Z_{\text{in}}$ in terms of dimensions and electrical parameters of the insulated probe and the finite biological body. Note that $R_{1n}(b)=0$ for the special case of a spherical antenna in free space; in this situation, (26) for the antenna impedance reduces to that given by Stratton and Chu [11].

Numerical results for Z_{in} computed from (26) are presented in the next section. It is important to note that this value for Z_{in} is actually an "edge" impedance defined at the surface of the metallic sphere; input impedances are normally measured, however, at the center ($r=0$) of a

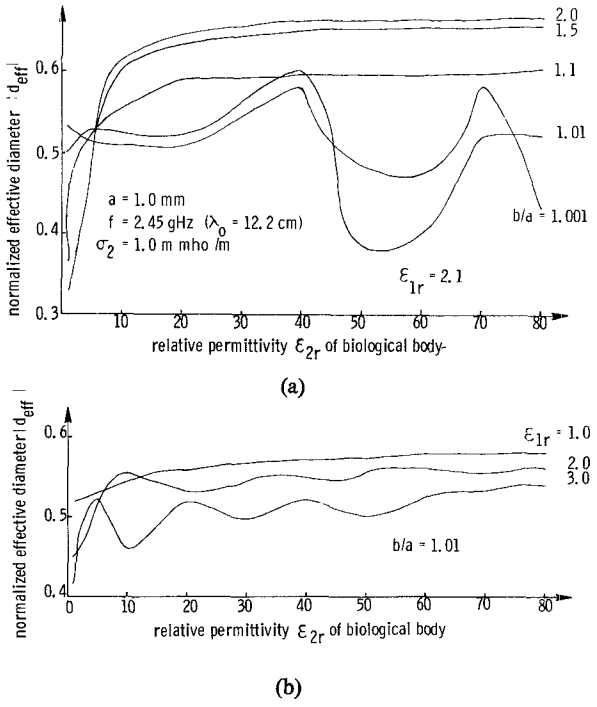

Fig. 2. Dependence of magnitude of normalized effective diameter $|d_{eff}|$ upon relative permittivity ϵ_{2r} of finite low-loss conducting biological body. (a) Variable parameter is b/a. (b) Variable parameter is ϵ_{1r}.

hemispherical antenna excited over a ground screen by a coaxial line. Edge impedances must therefore be appropriately transformed to the antenna center. Two methods for effecting this impedance transformation are described in [14] and are not repeated here.

V. Theoretical and Experimental Results

Representative numerical results, based on expressions for the effective diameter and equivalent impedance of the insulated, spherical electric field probe, are presented in this section. Included in the latter part of the section are comparisons between theoretical and experimentally measured impedances as well as experimental measurements of the power density distributions excited in saline models of finite biological bodies by an impressed plane-wave field.

Numerical results for the dependence of normalized effective diameter $|d_{eff}|$ upon relative permittivity ϵ_{2r} of a low-loss biological body are indicated in Fig. 2. Probe radius is $a=1.0$ mm and the frequency is $f=2.45$ GHz with remaining parameters specified in the figure. The parameter is b/a (insulation thickness) in Fig. 2(a), while ϵ_{1r} (insulation permittivity) is the parameter in Fig. 2(b). As b/a is varied from 1.001 (very thin coating) to 2.0 (relatively thick coating), it is observed that $|d_{eff}|$ becomes nearly independent of the body dielectric constant when $\epsilon_{2r} \gtrsim 10$, provided the insulating layer is adequately thick. It also indicates that $|d_{eff}|$ may vary greatly in biological tissues with dielectric constants lower than 10, such as fat or bone. Fig. 2(b) indicates that variations of $|d_{eff}|$ with body permittivity ϵ_{2r} are minimal for the smallest values of insulation permittivity $\epsilon_{1r} \approx 1$. Additional numerical computations show that d_{eff} is relatively insensitive to variations in conductivity σ_2 of the biological body. It is concluded that the effective diameter of a probe insulated by a thick layer of low-permittivity dielectric is minimally dependent upon electrical parameter variations of the biological body in which it is immersed if the dielectric constant of the body is greater than 10.

Numerical results for dependence of insulated spherical antenna impedance $Z_{eq}=Z_{in}$ upon dimensions and electrical parameters of the probe and body are presented in Figs. 3–5. Since the probe is always electrically small, its resistance $R_{eq}=R_{in}$ is very small relative to its reactance $X_{eq}=X_{in}$; numerical results for X_{eq} are therefore presented while those for R_{eq} are omitted. Probes of radius $a=1$ cm excited at frequency $f=600$ MHz are considered in each case (theoretical results compared with experimental measurements, for which these dimensions and frequency were convenient, later). Remaining dimensions and electrical parameters are specified in the figures.

The dependence of X_{eq} on radius c of the biological body is indicated in Fig. 3 as parameter b/a is varied from 1.1 to 3.0 with fixed insulation permittivity $\epsilon_{1r}=2.1$ (e.g., teflon). Lossy-dielectric body parameters are $\epsilon_{2r}=70$ and $\sigma_2=0.1$ mho/m. It is evident that X_{eq} varies strongly with c for small values of b/a but is relatively independent of body radius for thick insulation layers. For thin insulation, equivalent probe reactance X_{eq} (and Z_{eq}) changes rapidly and becomes very large, as shown by x^s on the figure, for small values of c; this corresponds to a situation where the probe is located near the boundary of a finite body. This latter observation explains the "edge difficulty" reported previously [7] during actual field measurements inside finite conducting bodies; the problem is associated with changes in probe calibration coefficient K (14) due to variations of Z_{eq} as the probe approaches a finite body boundary.

The effects of body dielectric constant ϵ_{2r} on X_{eq} are indicated in Fig. 4 with b/a varied as parameter from 1.0 (bare probe) to 3.0. The antenna, insulated by a layer with $\epsilon_{1r}=2.1$, is immersed in a low-loss body of radius $c=10$ cm and conductivity $\sigma_2=0.01$ mmho/m. Considerable variation of X_{eq} with ϵ_{2r} is evident for thin insulation with b/a between 1.0 (bare) and 1.1; this variation is significantly reduced by use of relatively thick dielectric coatings having b/a in the range of 1.5 to 3.0. Fig. 5 again displays the dependence of X_{eq} on ϵ_{2r} for the same probe and low-loss body ($\sigma_2=1.0$ mmho/m) except that the insulating layer with thickness $b/a=1.1$ has its dielectric constant varied as the parameter between $\epsilon_{1r}=1.0$ and $\epsilon_{1r}=10.0$. It is observed that larger values ϵ_{1r} lead to greater (percentage) variations in equivalent probe reactance (impedance) throughout the range of permittivities $\epsilon_{2r}>10$. In Figs. 4 and 5, X_{eq} was again found to vary greatly with ϵ_{2r} in the range of $\epsilon_{2r}<10$. This phenomenon may limit the applicability of an implantable electric field probe in biological tissues with low dielectric constants such as low-water content tissues. It is concluded that, to

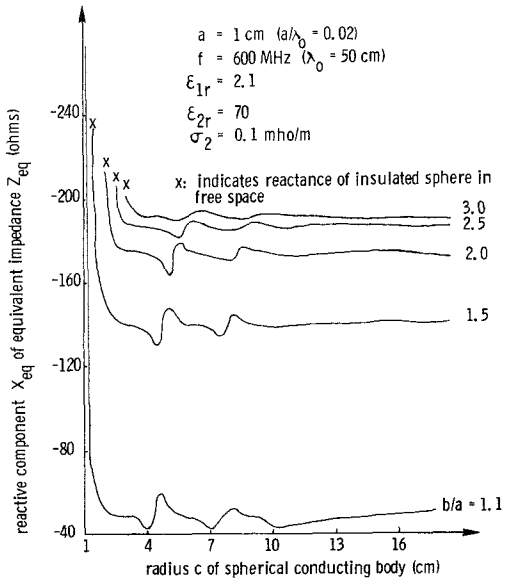

Fig. 3. Dependence of reactive component of equivalent probe impedance on radius of conducting spherical biological body.

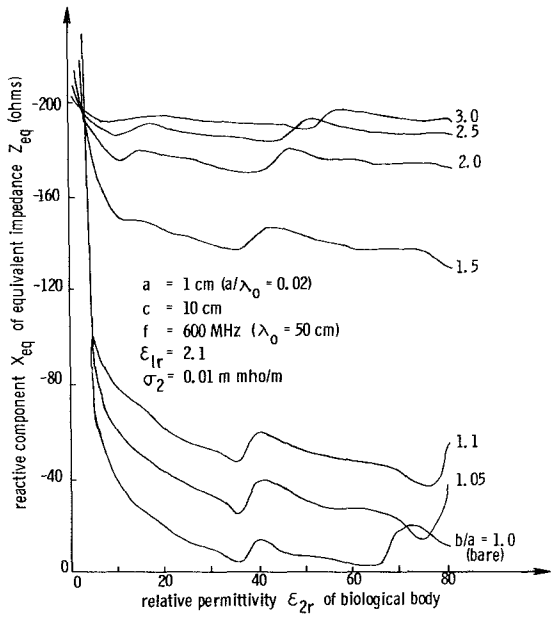

Fig. 4. Dependence of reactive component of equivalent probe impedance on relative permittivity ϵ_{2r} of low-loss conducting spherical biological body.

implement a probe which is minimally dependent upon local electrical parameter variations of the body in which it is immersed, the probe should be insulated by a dielectric coating having a maximum feasible thickness and a minimal (near unity) possible dielectric constant.

Numerical results discussed above were obtained primarily for low-loss bodies; variations of d_{eff} and Z_{eq} with body dimensions and electrical parameters are most severe for such bodies with small dissipation. Extensive numerical calculations have indicated, however, that neither d_{eff} nor Z_{eq} of the insulated spherical probe are significantly effected by conductivity variations in the surrounding body. Variations of both resistive and reactive components of equivalent impedance $Z_{\text{eq}} = R_{\text{eq}} + jX_{\text{eq}}$ with conductivity σ_2 of the biological body are indicated in Fig. 6. Radii of the antenna and body are $a = 1.0$ cm and $c = 5.0$ cm, dielectric constants of insulation and body are $\epsilon_{1r} = 2.1$ and $\epsilon_{2r} = 50$, and the excitation frequency is $f = 600$ MHz; insulation thickness is varied as the parameter from $b/a = 1.1$ to $b/a = 2.0$. It is noted that, for thick

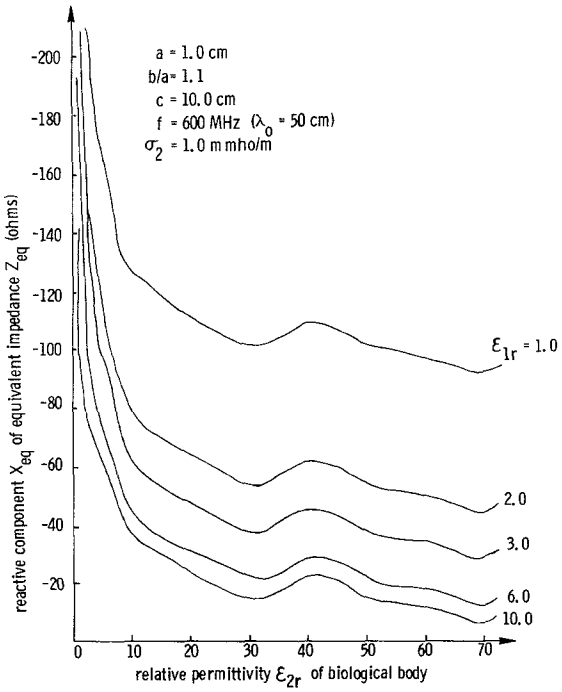

Fig. 5. Dependence of reactive component of equivalent probe impedance on relative permittivity ϵ_{2r} of low-loss conducting spherical biological body.

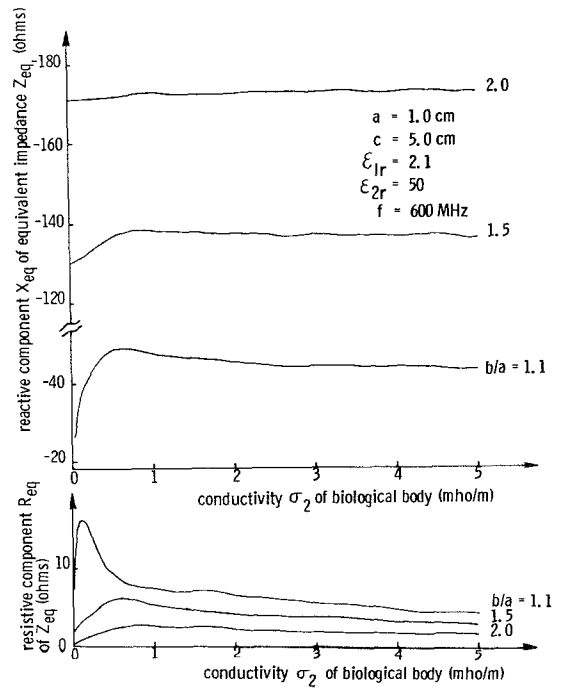

Fig. 6. Dependence of equivalent probe impedance $Z_{\text{eq}} = R_{\text{eq}} + jX_{\text{eq}}$ on conductivity σ_2 of conducting spherical biological body (insulation thickness as parameter).

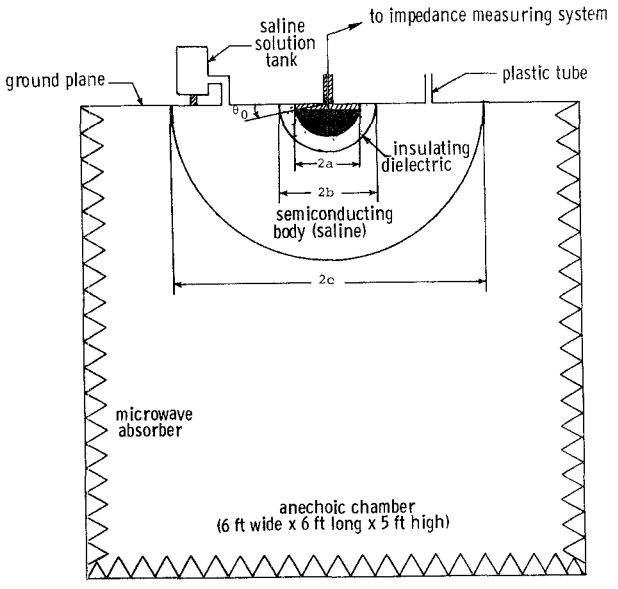

Fig. 7. Experimental arrangement of insulated spherical antenna immersed in semiconducting body below conducting ground plane in anechoic chamber.

insulation coatings, both R_{eq} and X_{eq} become relatively independent of conductivity for the finite body in which the probe is embedded.

Experimental measurements were made on a metallic hemispherical antenna excited over a conducting ground plane by a coaxial transmission system and radiating into an anechoic chamber as indicated in Fig. 7. Insulation consists of a concentric hemispherical nylon layer, while the insulated probe is immersed in a hemispherical volume of saline solution again located concentric with the antenna. Input resistance $R_{eq}=R_{in}$ to the electrically small probe is very small, resulting in high standing-wave ratios (SWR's) on the input transmission system; conventional slotted line measurements of $Z_{eq}=Z_{in}$ are thus difficult and relatively inaccurate. The relatively new E–H probe technique was therefore utilized to implement Z_{in} measurements. Ratio V/I at the probe location is calculated from vector voltimeter measurements of calibrated E–H probe response; this measured impedance is finally transformed to the antenna terminals to evaluate Z_{in}. Details of the technique have been reported elsewhere [15].

Theoretical and experimentally measured input reactances X_{in} to a hemispherical antenna of radius $a=1.1$ cm embedded in a conducting hemispherical body with radius $c=5.5$ cm are presented in Table I. The body is modeled by air, distilled H_2O, and saline solutions of varying normality as indicated. Nylon insulation with dielectric constant $\epsilon_{1r}\approx 3.0$ is utilized with radii of $b=1.2$, 1.5, and 6.1 cm. Electrical parameters of the saline were calculated for frequency $f=600$ MHz ($\lambda_0=50$ cm) at temperature $T=20°C$. Agreement between theoretical reactances and those measured experimentally is observed to be very good. Thin coatings, i.e., $b=1.21$ cm, lead to considerable variation of reactance X_{in} (and consequently Z_{in}) with parameters of the medium surrounding the insulated

TABLE I

THEORETICAL AND EXPERIMENTALLY MEASURED INPUT REACTANCES X_{in} TO AN INSULATED HEMISPHERICAL ANTENNA IMMERSED IN A FINITE HEMISPHERICAL EXTERNAL (BIOLOGICAL BODY) MEDIUM ($a=1.1$ cm, $c=5.5$ cm, $f=600$ MHz, $\epsilon_{1r}\approx 3.0$, $T=20°C$)

external (biological) medium	parameters		X_{in} (ohms) ($b=1.21$ cm)		X_{in} (ohms) ($b=1.5$ cm)		X_{in} (ohms) ($b=3.1$ cm)	
	ϵ_2/ϵ_0	σ_2 mho/m	theory	exp	theory	exp.	theory	exp
air	1.0	0.0	-20.99	-19.5	-19.34	-18.8	-22.54	-22.0
dist. H_2O	79.9	0.095	-9.06	-11.5	-14.89	-14.6	-21.59	-21.2
0.5 N saline	70.9	4.52	-8.23	-10.1	-14.57	-14.1	-21.77	-21.5
1.0 N saline	62.9	7.74	-8.07	-8.0	-14.55	-14.0	-21.75	-21.6
1.5 N saline	56.9	10.8	-8.06	-8.8	-14.55	-14.0	-21.75	-21.5
2.0 N saline	51.0	13.8	-8.08	-9.2	-14.56	-14.2	-21.75	-21.5

TABLE II

EXPERIMENTALLY MEASURED INPUT IMPEDANCES TO A DIELECTRIC COATED HEMISPHERICAL ANTENNA AT VARIOUS LOCATIONS IN A FINITE HEMISPHERICAL CONDUCTING BODY ($a=1.1$ cm, $c=5.5$ cm, $f=600$ MHz, $\epsilon_{1r}\approx 3.0$, $\epsilon_{2r}=77.9$, $\sigma_2=0.925$ mho/m, $T=20°C$)

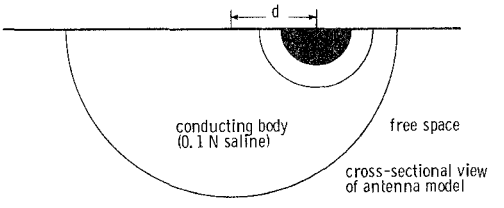

d (cm)	input impedance Z_{in} (ohms)		
	$b=1.2$ cm	$b=1.6$ cm	$b=2.2$ cm
0.0	1.0 - j10.5 (theory 1.0 - j10.0)	0.8 - j16.0 (theory 0.2 - j15.6)	0.5 - j19.0 (theory 0.13 - j18.5)
2.6	1.3 - j14.2	1.0 - j16.6	0.6 - j19.0
3.3	1.5 - j15.0	1.0 - j16.7	0.7 - j19.0

probe. X_{in} is relatively independent of conducting body parameters when thick insulation layers, i.e., $b=3.1$ cm, are utilized. These results are consistent with theoretical ones discussed earlier.

Experimental measurements of impedance Z_{in} to the same insulated spherical probe are presented in Table II when the center of the hemispherical antenna is displaced by distance d from the conducting-body center. These results demonstrate the effects of finite body dimensions and relative probe location upon the equivalent probe impedance $Z_{eq}=Z_{in}$. The finite conducting body consists of 0.1N saline solution and impedances are tabulated for three insulation thicknesses $b=1.2$, 1.6, and 2.2 cm and three displacements $d=0.0$, 2.6, and 3.3 cm. Results of Table II demonstrate that impedances of the thickly insulated probe are essentially independent of its location in the finite body; for this case, the body can be approximated as infinite in extent. Thin dielectric coatings, however, lead to significant impedance variations as the probe is moved about in a finite body.

A spherical probe insulated by a dielectric coating and loaded by a microwave detector diode was constructed to implement the measurement of actual power density dis-

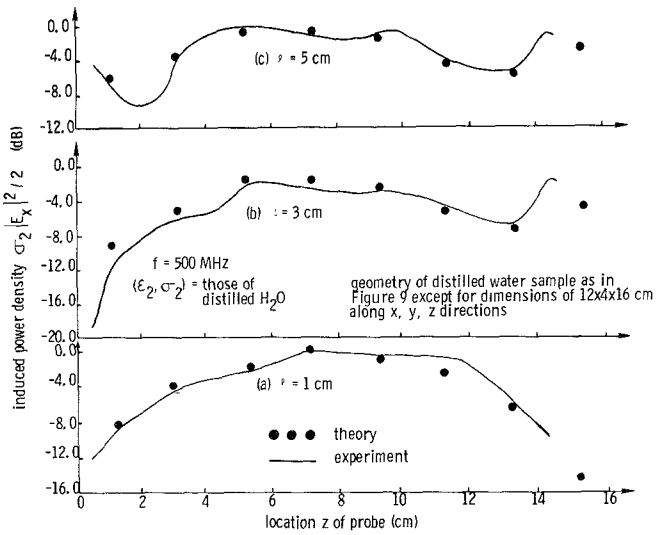

Fig. 8. Comparison of calculated and measured induced power density ($|E_x|^2$) distributions at distance below upper surface of rectangular volume of distilled H_2O (geometry as in Fig. 9).

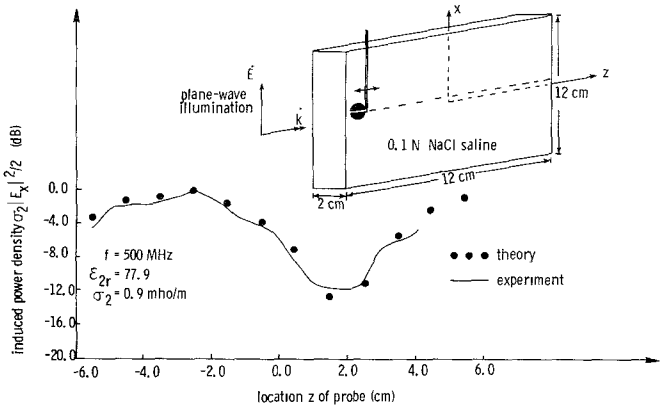

Fig. 9. Comparison of calculated and measured induced power density ($|E_x|^2$) distributions 0.5 cm above the center of a finite volume of saline solution simulating a biological body.

tributions induced in a finite conducting body by an impressed plane-wave field. Details are included in [14] while measured power distributions are compared here with theoretical predictions in Figs. 8 and 9. Measurements were made at frequency $f=600$ MHz by a probe with radii $a=0.5$ cm and $b=0.6$ cm insulated by a Plexiglas layer having $\epsilon_{1r}\approx 3.0$. Fig. 8 indicates the measured distribution of induced power density ($|\vec{E}|^2$ in decibels) inside a $16\times 12\times 4$ cm finite volume of distilled H_2O as a function of axial location z. Distance l from the probe center to the top body surface is varied ($l=1$, 3, and 5 cm) as parameter. Theoretical predictions, indicated by dots in the figure, are obtained by the existing tensor-integral-equation technique and moment-method numerical solution [16]. It is noted that, in this theoretical method, the volume is subdivided into a number of cells and the induced field is assumed to be constant throughout each cell. Thus the theoretical results indicated by dots represent approximately the average values of induced power densities inside volume cells, and the theoretical results are represented by a series of rectangular functions instead of a smooth curve. Similar measurements for the dependence of induced power density upon axial location z in a $12\times 12\times 2$ cm volume (body model) of $0.1N$ saline are indicated in Fig. 9; comparisons with theoretical predictions are again included. Agreement between theoretical predictions and experimental measurements is good in both cases. Minor discrepancies can be attributed to incomplete convergence of the numerical solution and inherent experimental errors associated with relatively large probe dimensions and its connections with measurement apparatus. It is important to note that the "edge difficulty" encountered in [7] has been overcome (theory and experiment agree well at body boundaries) by insulating the probe with a dielectric layer of adequate thickness.

VI. Conclusion and Discussion

Anomalous electric-field probe responses and associated measured field errors can result due to the dependence of the probe calibration factor upon the location of the probe in a finite heterogeneous biological body. Calibration coefficient variations result from the location dependence of probe effective length and equivalent impedance; these equivalent-circuit parameters can depend strongly upon local values of the body electrical parameters and the proximity of the probe to finite body boundaries. It has been demonstrated, both analytically and experimentally, that an electric field probe with a relatively constant calibration factor can be implemented by insulating the metallic probe with a thick dielectric coating of low permittivity. The effective diameter and equivalent impedance of a spherical probe become relatively independent of finite size and electrical parameters of the body in which it is immersed when the insulation-to-probe diameter ratio exceeds $b/a\approx 1.5$ with insulation of dielectric constant $\epsilon_{1r}\approx 2.0$. Agreement of actual measurements for the field distribution in a simulated finite biological body, obtained using such an insulated probe, with theoretical predictions confirms this conclusion.

A spherically symmetrical geometry was adapted in the present study in the interest of obtaining an exact solution. Only with accurate theoretical results, though based on an idealized geometry, can general characteristics of an insulated electric field probe in a finite biological body be carefully examined. Since the main findings of the present study are rather geometry independent, it appears that the results of the present study can be applied to systems without spherical symmetry. This point was verified by the experimental study.

The main advantages of using an implantable electric field probe over a temperature probe are its capability of measuring a low induced field and its ability of measuring each component of the induced electric field separately. However, it also has disadvantages such as the limitation

of using it in regions with low dielectric constants and the difficulty of designing an interference-free lead wire system for the probe. An implantable electric field probe with an interference-free lead-wire system has subsequently been developed by our laboratory. This information will be published in a future paper.

References

[1] C. C. Johnson and A. W. Guy, "Nonionizing electromagnetic wave effects in biological materials and systems," *Proc. IEEE*, vol. 60, pp. 692–718, June 1972.

[2] C. C. Johnson, "Research needs for establishing a radio frequency electromagnetic radiation safety standard," *J. Microwave Power*, vol. 8, pp. 367–388, Nov. 1973.

[3] S. M Michaelson, "Review of a program to assess the effects on man from exposure to microwaves," *J. Microwave Power*, vol. 9, June 1974.

[4] H. Bassen, M. Swicord, and J. Abita, "A miniature broad-band electric field probe," *Ann. N.Y. Acad. Sci.*, vol. 247, pp. 481–493, 1975.

[5] A. Cheung, H. Bassen, M. Swicord, and D. Witters, "Experimental calibration of a miniature electric field probe within simulated muscular tissues," in *Proc. 1975 URSI Bioeffects Symp.*, to be published.

[6] G. Smith, "A comparison of electrically-short bare and insulated probes for measuring the local radio frequency electric field in biological systems," *IEEE Trans. Biomed. Eng.*, vol. ME-22, pp. 477–783, Nov. 1975.

[7] B. S. Guru and K. M. Chen, "Experimental and theoretical studies on electromagnetic fields induced inside finite biological bodies," *IEEE Trans. Microwave Theory Tech.*, vol. MTT-24, pp. 433–440, July 1976.

[8] H. Bassen, W. Herman, and R. Ross, "EM probe with fiber optic telemetry system," *Microwave J.*, pp. 35–47, Apr. 1977.

[9] H. Bassen, A. Cheung, and K. M. Chen, "Comments on 'Experimental and theoretical studies on electromagnetic fields induced inside finite biological bodies,'" *IEEE Trans. Microwave Theory Tech.*, vol. MTT-25, pp. 623–624, July 1977.

[10] R. W. P. King, "The many faces of the insulated antenna," *Proc. IEEE*, vol. 64, 228–238, Feb. 1976.

[11] J. A. Stratton and L. J. Chu, "Forced oscillation of a conducting sphere," *J. Appl. Phys.*, vol. 12, pp. 230–248, Mar. 1941.

[12] M. Abramowitz and I. A. Stegun, *Handbook of Mathematical Functions*. New York: Dover, 1970.

[13] L. Infeld, "The influence of the width of the gap upon the theory of antennas," *Quart. Appl. Math.*, vol. V, pp. 113–132, July 1947.

[14] S. H. Mousavinezhad, "Implantable electromagnetic field probes in finite biological bodies," Michigan State Univ., East Lansing, Ph.D. disertation, 1977.

[15] H. Mousavinezhad, K. M. Chen, and D. P. Nyquist, "Implantable field probes in finite biological bodies," presented at the 1976 Int. IEEE/AP-S Symp., Univ. of Massachusetts, Amherst, Oct. 1976.

[16] D. Livesay and K. M. Chen, "EM field induced inside arbitrarily-shaped biological bodies," *IEEE Trans Microwave Theory Tech.*, vol. MTT-22, pp. 1273–1280, Dec. 1974.

Heat Potential Distribution in an Inhomogeneous Spherical Model of a Cranial Structure Exposed to Microwaves Due to Loop or Dipole Antennas

ALTUNKAN HIZAL AND YAHYA KEMAL BAYKAL

Abstract—**An inhomogeneous spherical model of a 3.3-cm radius cranial structure is assumed to be placed symmetrically in the near field of a small loop antenna or an electrical dipole antenna at 3 GHz. The transitions between the layers are taken to be sharp but sinusoidal. Calculations of the heat potential are performed using a spherical wave expansion technique in which linear differential equations are solved for the unknown multipole coefficients. The results are also compared with the plane-wave excitations. It is seen that a more uniform distribution of the heat potential occurs for the dipole antenna excitation which is also similar to the *E*-plane distribution in the case of plane-wave excitation. For the loop excitation, a significant hot spot occurs near the center of the structure.**

Manuscript received July 8, 1977; revised February 21, 1978.

A Hizal is with the Electrical Engineering Department, Middle East Technical University, Ankara, Turkey.

Y. K. Baykal was with the Electrical Engineering Department, Middle East Technical University, Ankara, Turkey. He is now at Northwestern University, Evanston, IL 60201.

I. Introduction

THE PREDICTION of the heat potential distribution in a cranial structure excited by a microwave radiation is of interest for the purposes of medical treatment and searching out the radiation hazards. For this purpose, multilayered spherical models [1], [2] irradiated by a plane wave have been analyzed. It is found that a nonuniform

0018-9480/78/0800-0607$00.75